

# Multitask quantum thermal machines and cooperative effects

Jincheng Lu,<sup>1</sup> Zi Wang,<sup>2</sup> Rongqian Wang,<sup>3</sup> Jiebin Peng,<sup>4</sup> Chen Wang,<sup>5,\*</sup> and Jian-Hua Jiang<sup>3,†</sup>

<sup>1</sup>*Jiangsu Key Laboratory of Micro and Nano Heat Fluid Flow Technology and Energy Application, School of Physical Science and Technology, Suzhou University of Science and Technology, Suzhou, 215009, China*

<sup>2</sup>*Center for Phononics and Thermal Energy Science, China-EU Joint Lab on Nanophononics, Shanghai Key Laboratory of Special Artificial Microstructure Materials and Technology, School of Physics Science and Engineering, Tongji University, Shanghai 200092, China*

<sup>3</sup>*Institute of theoretical and applied physics & School of physical science and technology & Collaborative Innovation Center of Suzhou Nano Science and Technology, Soochow University, Suzhou 215006, China.*

<sup>4</sup>*School of Physics and Optoelectronic Engineering, Guangdong University of Technology, Guangzhou 510006, Guangdong Province, China*

<sup>5</sup>*Department of Physics, Zhejiang Normal University, Jinhua, Zhejiang 321004, China*

(Dated: September 20, 2022)

Including phonon-assisted inelastic process in thermoelectric devices is able to enhance the performance of nonequilibrium work extraction. In this work, we demonstrate that inelastic phonon-thermoelectric devices have a fertile functionality diagram, where particle current and phononic heat currents are coupled and fueled by chemical potential difference. Such devices can simultaneously perform multiple tasks, e.g., heat engines, refrigerators, and heat pumps. Guided by the entropy production, we mainly study the efficiencies and coefficients of performance of multitask quantum thermal machines, where the roles of the inelastic scattering process and multiple biases in multiterminal setups are emphasized. Specifically, in a three-terminal double-quantum-dot setup with a tunable gate, we show that it efficiently performs two useful tasks due to the phonon-assisted inelastic process. Moreover, the cooperation between the longitudinal and transverse thermoelectric effects in the three-terminal thermoelectric systems leads to markedly improved performance of the thermal machines. While for the four-terminal four-quantum-dot thermoelectric setup, we find that additional thermodynamic affinity furnishes the system with both enriched functionality and enhanced efficiency. Our work provides insights into optimizing phonon-thermoelectric devices.

## I. INTRODUCTION

Understanding the performance of thermoelectric transport at the nanoscale is of significant importance for its potential applications in quantum technology [1–5]. Much effort has been devoted to achieving high efficiency and coefficient of performance in thermoelectric nanodevices both theoretically [6–9] and experimentally [10, 11], which mainly originate from the elastic transport processes [12–17]. Interestingly, Mahan and Sofo proposed the “best thermoelectrics” by using conductors with very narrow energy bands to reduce the thermal conductivity based on the Wiedemann-Franz law [18]. However, it was recently discovered that phonon thermal transport will inevitably suppress the figure of merit, and output power in the zero band width limit [19]. The carrier of particle and heat current for the elastic transport processes is electrons, so it is impossible to spatially separate them. In contrast, it may be available to realize such separation of heat and charge currents in inelastic transport processes [20].

Recently, another fundamental category, i.e., inelastic transport processes, has been explored [21–29]. One exciting perspective is that the inclusion of an additional terminal to “decouple” the particle and heat currents may significantly improve thermoelectric efficiency. Until now, a vast of valuable works have been carried out to study inelastic transport in thermoelectric systems, e.g., Coulomb-coupled quantum dot (QD) systems [30, 31], metal-superconductor junctions [32], and boson-assisted thermoelectric devices [33–36]. However, the study of multiterminal energy conversion and transfer is still in its infancy, in which the thermodynamic machine usually performs a single task, such as refrigerators [37–39], heat pumps [40–43], or the heat engines [44–48]. Intriguingly, as proposed by Entin-Wohlman *et al.* [49] and Manzano *et al.* [50], a three-terminal device is considered as a hybrid thermal machine, which performs multiple efficient tasks simultaneously by introducing a reference temperature. Consequently, the thermoelectric effect accompanied by one electric current and two heat currents, is analyzed.

In this work, we give a universal exergy efficiency without relying on the particular reference temperature, based on the concept of entropy production. We show that inelastic thermoelectric devices with multiple elec-

\* Corresponding author: wangchen@zjnu.cn

† Corresponding author: jianhua.jiang@suda.edu.cn

tric currents and/or multiple heat currents can be nominated as hybrid thermal machines [51], i.e., devices concurrently performing multiple useful tasks. Specifically, we desire to analyze different thermoelectric devices performing distinct tasks, e.g., heat engines, refrigerators, and heat pumps. When a system connects to multiple reservoirs, the entropy production rate of the whole system is described as  $\dot{S}_{\text{tot}} = \sum_{i=1}^N \dot{S}_i$ , where  $\dot{S}_i$  is the entropy production rate of the  $i$ th reservoir [52]. If we denote  $T$  as the temperature of a reservoir, which is the intermediate temperature compared with others (instead of deliberately introducing a reference temperature), the entropy production can be decomposed into [52, 53]

$$T\dot{S}_{\text{tot}} = T \sum_{v=1}^N \dot{S}_v = \sum_{v=1}^N I_v A_v, \quad (1)$$

where  $I_v$  is the current and  $A_v$  is the corresponding affinity. Then, the exergy efficiency is defined as the ratio of all the entropy decrease terms (the inputs) to all the entropy increase terms (the outputs) [50, 54–56]

$$\phi = -\frac{\sum_v^- \dot{S}_v}{\sum_v^+ \dot{S}_v} \leq 1, \quad (2)$$

where  $\sum_v^\pm \dot{S}_v$  denotes the sum over the positive and negative terms of the rates, respectively. According to the second law of thermodynamics, the exergy efficiency is bounded via  $\phi \leq 1$  [57]. In Eqs. (1) and (2), we use the temperature of a reservoir  $T$  in the middle to characterize whether a process is negative entropy production (useful) or positive entropy production (useless). In this way, we avoid the situations that different choices of reference temperature lead to different conclusions, and may even violate the second law of thermodynamics.

The exergy efficiency [Eq. (2)] has been extensively studied both at the equilibrium and nonequilibrium regimes [55, 58, 59]. Interestingly, the relation between the exergy efficiency  $\phi$  and conventional efficiency  $\eta = W/Q$  ( $W$  and  $Q$  are the output work and input heat) is obtained as [58]

$$\phi = \eta/\eta_C, \quad (3)$$

where  $\eta_C = 1 - T_c/T_h$  is the Carnot efficiency, and  $T_c$  and  $T_h$  are the temperatures of the cold and hot reservoirs, respectively. The important issue in quantum thermodynamics is to find out the optimal efficiency and the corresponding maximal power of thermal machines.

While considering energy conversion, thermoelectric cooperative effects have been demonstrated to be an effective way to improve conversion efficiency (figure of merit) [58, 60–62]. As shown in Fig. 1, the thermal machine connects to two input currents and one output current. And there are two thermoelectric effects

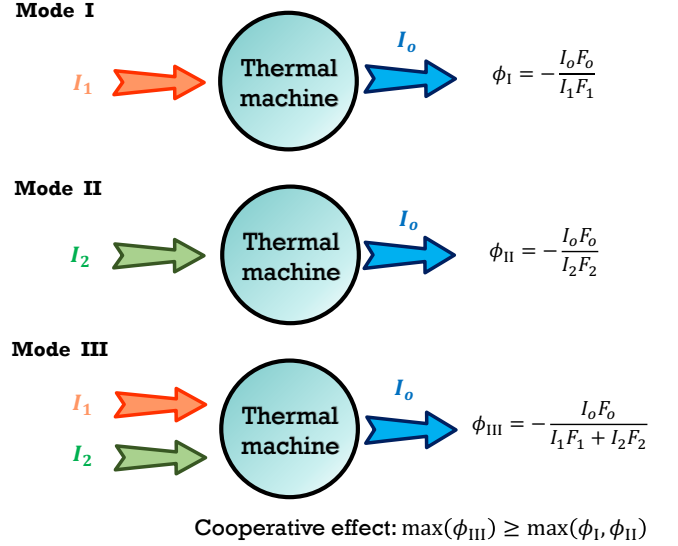


FIG. 1. Schematic illustration of thermoelectric cooperative effects in quantum thermal machine.  $I_i$  ( $i = 1, 2$ ) denotes the input current and  $I_o$  is the output current,  $F_i$  is the corresponding force.  $\phi_i$  ( $i = \text{I, II, III}$ ) is the exergy efficiency of the thermal machine.

associated with different chemical potentials and/or temperature gradients. The essence of cooperative effect is to modulate the input currents through regulating the thermodynamic forces. For instance, there are only one input current in mode I and mode II, while mode III has two input currents. It is found that the exergy efficiency of mode III can be greater than mode I and II, i.e.,  $\max(\phi_{\text{III}}) \geq \max(\phi_{\text{I}}, \phi_{\text{II}})$ .

In the work, we primarily examine the general theoretical framework of multiterminal devices, i.e., double QDs three-terminal system comprising two electronic terminals and a phonon bath (Sec. II) and four-QD four-terminal system (Sec. III), defines the particle and heat currents and the corresponding thermodynamic driving forces, and uses those quantities to reexpress the efficiencies of the thermal machine for different tasks. We also discuss thermodynamic multitasks of the various setups in the linear response, based on the Onsager formalism. Finally section IV is devoted to the conclusions. We also discuss the performance of three-terminal single-level QD system that perform multiple useful tasks simultaneously in Appendix A. Throughout this work, we set electron charge  $e \equiv 1$  and Planck constant  $\hbar \equiv 1$ .

## II. THE THREE-TERMINAL DOUBLE QDS DEVICE

In this section we will present a generic inelastic transport model to illustrate multitasks of hybrid thermal machines. The simplest nontrivial geometry configuration for inelastic transport is the three-terminal system, where energy absorbed/emitted by the electron is assisted by a third phonon bath, differing from the left reservoir and right reservoir. This model is characterized as a hopping double QDs model [33, 36, 46, 63, 64]. At linear thermoelectric response regime, one remarkable feature of double QDs is that the three-terminal system exhibits a large thermopower and high figure of merit [33]. Moreover, it is found that nonlinear thermoelectric transport can further enhance energy efficiency and output power under nonlinear driving sources [46]. Here, we mainly focus on the efficiencies and coefficients of performance of multi-task three-terminal inelastic phonon-thermoelectric device.

### A. The basic setup and currents

The three-terminal double QDs device consists of the left reservoir, the right reservoir, and a phonon bath, as schematically depicted in Fig. 2. The QDs are labeled by  $L$  and  $R$  with tunable energy levels  $E_L$  and  $E_R$ . An electron leaves the left QD and hops to the right QD, which is simultaneously assisted by one phonon from the phonon bath (with temperature  $T_{ph}$ ). The Hamiltonian of the double-QDs device is  $\hat{H} = \hat{H}_{DQD} + \hat{H}_{e-ph} + \hat{H}_{lead} + \hat{H}_{tun} + \hat{H}_{ph}$ , with  $\hat{H}_{DQD} = \sum_{i=L,R} E_i \hat{b}_i^\dagger \hat{b}_i + t(\hat{b}_L^\dagger \hat{b}_R + \text{H.c.})$ ,  $\hat{H}_{e-ph} = \sum_q \lambda_q \hat{b}_L^\dagger \hat{b}_R (\hat{d}_q + \hat{d}_q^\dagger) + \text{H.c.}$ ,  $\hat{H}_{ph} = \sum_q \omega_q \hat{d}_q^\dagger \hat{d}_q$ ,  $\hat{H}_{lead} = \sum_{j=L,R} \sum_k \varepsilon_{j,k} \hat{b}_{j,k}^\dagger \hat{b}_{j,k}$ , and  $\hat{H}_{tun} = \sum_k V_{L,k} \hat{b}_L^\dagger \hat{b}_{L,k} + \sum_k V_{R,k} \hat{b}_R^\dagger \hat{b}_{R,k} + \text{H.c.}$ , where  $\hat{b}_i^\dagger$  ( $\hat{b}_i$ ) is the creation (annihilation) operator of electron in the  $i$  QD, and  $E_i$  is the QD energy,  $t$  is the tunneling between the two QDs,  $\gamma_L$  ( $\gamma_R$ ) is the coupling between the QD and the left (right) reservoir,  $\lambda_q$  is the strength of electron-phonon interaction, and  $\hat{d}_q^\dagger$  ( $\hat{d}_q$ ) is the creation (annihilation) operator of phonon with the frequency  $\omega_q$ .

There exist particle  $I_p^i$  ( $i = L, R$ ), energy  $I_E^i$  ( $i = L, R, ph$ ), and heat  $I_Q^i$  ( $i = L, R, ph$ ) currents out of the  $i$ -th reservoir, which are denoted by grey lines with arrows in Fig. 2 [21, 35]. Accordingly, the electric and phononic heat currents are given by  $I_Q^i = I_E^i - \mu_i I_p^i$  ( $i = L, R$ ) and  $I_Q^{ph} = I_E^{ph}$ . We define that the current  $I_i$  is positive when flowing towards the hybrid quantum system. Moreover, the energy conversion leads to the relation  $I_E^L + I_E^R + I_Q^{ph} = 0$  [21], while the particles conversion results in  $I_p^L + I_p^R = 0$ . Moreover, The entropy production relation of the system is given by [65]

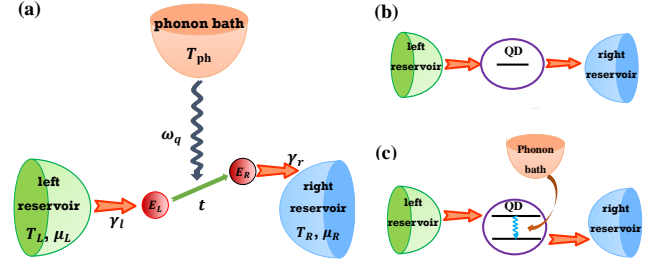


FIG. 2. Illustration of three-terminal double QD system. An electron left the left reservoir into the left QD (with energy  $E_L$ ) hops to the right QD (with a energy  $E_R$ ) as assisted by a phonon from the phonon bath (with temperature  $T_{ph}$ ). The electron then tunnels into the right reservoir from the right QD. The electrochemical potential and temperature of the left reservoir (right reservoir) are  $\mu_L$  and  $T_L$  ( $\mu_R$  and  $T_R$ ), respectively.  $\gamma_{l/r}$  are the hybridization energies of the QDs to the left/right reservoir, respectively. Illustration of (b) elastic, (c) inelastic thermoelectric transport.

$-\dot{S}_{tot} = I_Q^L/T_L + I_Q^R/T_R + I_Q^{ph}/T_{ph}$ . Combining the particle and energy currents conservation relations, the entropy production rate can be reexpressed as

$$T_L \frac{dS_{tot}}{dt} = I_p^R A_p^R + I_Q^R A_Q^R + I_Q^{ph} A_Q^{ph}, \quad (4)$$

where  $A_p^R = \mu_R - \mu_L$ ,  $A_Q^R = 1 - \frac{T_L}{T_R}$ , and  $A_Q^{ph} = 1 - \frac{T_L}{T_{ph}}$ . Based on the Fermi golden rule [33], one is able to obtain the contribution of inelastic processes to the heat currents

$$\begin{aligned} I_Q^{L,inel} &= (E_L - \mu_L) I_p^L, \\ I_Q^{R,inel} &= -(E_R - \mu_R) I_p^R, \\ I_Q^{ph,inel} &= (E_R - E_L) I_p^L. \end{aligned} \quad (5)$$

Here  $I_p^{L,inel} = \Gamma_{l \rightarrow r} - \Gamma_{r \rightarrow l}$  with  $\Gamma_{l \rightarrow r} \equiv \gamma_{e-ph} f_l (1 - f_r) N_p^-$  and  $\Gamma_{r \rightarrow l} \equiv \gamma_{e-ph} f_r (1 - f_l) N_p^+$ .  $N_p^\pm = N_B + \frac{1}{2} \pm \frac{1}{2} \text{sgn}(E_R - E_L)$  with  $N_B \equiv [\exp(|E_R - E_L|/T_{ph}) - 1]^{-1}$  being the Bose-Einstein distribution for phonons.  $\gamma_{e-ph} = |\lambda_q|^2 v_{ph}$ , where  $v_{ph}$  denotes the phonon density of states. In the following, we assume that  $f_i \approx \exp[(E_i - \mu_i)/k_B T_i] + 1^{-1}$ , where  $f_i$  ( $i = L, R$ ) is the Fermi distribution function for the  $i$ -th electric reservoir. In Fig. 2(c), we can find that the inelastic process mainly results from the electron-phonon interaction processes, which involve the collaborative transport between three reservoirs.

In contrast, the contribution of elastic processes [see Fig. 2(b)] does not involve the electron-phonon scattering. The electron only tunnels from the left electronic reservoir to the right one, and vice versa. The elastic currents can be obtained through the Landauer-Buttiker

formula [66]

$$\begin{aligned} I_e^{L,\text{el}} &= \int \frac{dE}{2\pi} \mathcal{T}(E) [f_L(E) - f_R(E)], \\ I_Q^{L,\text{el}} &= \int \frac{dE}{2\pi} (E - \mu_L) \mathcal{T}(E) [f_L(E) - f_R(E)], \\ I_Q^{\text{ph},\text{el}} &= 0, \end{aligned} \quad (6)$$

where  $\mathcal{T}(E)$  is the transmission function and can be obtained from the Caroli formula [65]. Note that elastic processes do not contribute to the heat current  $I_Q^{\text{ph}}$ . For simplicity we assume that tunneling rates  $\gamma_L = \gamma_R$  and energy independent in this work. Both elastic and inelastic processes contribute to nonequilibrium currents, i.e.,  $I = I^{\text{el}} + I^{\text{inel}}$ .

Then the power done by the reservoirs for the device is expressed as [21, 49]

$$\dot{W} = I_p^R \Delta\mu, \quad (7)$$

where  $\Delta\mu = \mu_R - \mu_L \equiv A_p^R$  is the chemical potential difference. By default, we will consider the temperatures as  $T_R < T_L < T_{\text{ph}}$ , where the temperature of the left reservoir is chosen as the reference temperature. Hence, it should be easier to characterize which task the system is performing.

### B. The efficiency of power production, cooling, and heating by performing a single task

In this part, we introduce the exergy efficiencies for three thermodynamic operations: heat engines, refrigerators, and heat pumps. The exergy efficiency is a dimensionless ratio where the device's output exergy dividing the input one. For example, heat engines converts temperature gradients to extract useful work, e.g., thermoelectric engine [67]. In such a thermoelectric heat engine, the heat current absorbed from the hot reservoir (phonon bath) is used to drive particle current against the chemical potential bias  $\Delta\mu$ , i.e.,  $I_Q^R < 0$ ,  $I_Q^{\text{ph}} > 0$ , and  $\dot{W} < 0$ . According to the Eq. (2), the efficiency of the thermoelectric heat engine is given by

$$\phi_E = \frac{-\dot{W}}{I_Q^R A_Q^R + I_Q^{\text{ph}} A_Q^{\text{ph}}}. \quad (8)$$

Based on the above relation ( $\phi_E > 0$ ), we know that the negative entropy production associated with power done by the reservoirs,  $\dot{W} < 0$ , is compensated by the positive entropy production of  $I_Q^R A_Q^R + I_Q^{\text{ph}} A_Q^{\text{ph}}$ , in agreement with Kedem and Caplan [68].

While for the refrigerator operation, it appears when heat current flows out of the coldest reservoir ( $I_Q^R > 0$ ),

but no other useful task is performed (i.e.,  $I_Q^{\text{ph}} > 0$  and  $\dot{W} > 0$ ). Such efficiency is also termed as the coefficient of performance, defined as

$$\phi_R = \frac{-I_Q^R A_Q^R}{I_Q^{\text{ph}} A_Q^{\text{ph}} + \dot{W}}. \quad (9)$$

The third type of thermal operations is the heat pump, which is characterized as heat current flowing into the hot reservoir ( $I_Q^{\text{ph}} < 0$ ), but no other useful task being performed ( $I_Q^R < 0$  and  $\dot{W} > 0$ ). For the heat pump, we obtain [69],

$$\phi_P = \frac{-I_Q^{\text{ph}} A_Q^{\text{ph}}}{I_Q^R A_Q^R + \dot{W}}. \quad (10)$$

From the above discussion, we know that if we ignore the inelastic scattering processes, the heat current involved with the phonon bath becomes vanishing. The whole entropy production is simplified to  $T_L \frac{dS_{\text{tot}}^{\text{el}}}{dt} = I_p^{R,\text{el}} A_p^R + I_Q^{R,\text{el}} A_Q^R$ . And the three-terminal setup is reduced to the two-terminal one. Hence, it is obvious to demonstrate that the thermal machines can only perform single task. In other words, only when multiple terminals cooperate with each other, the thermal machine may perform multiple useful tasks simultaneously, e.g., the third terminal is either a phononic or an electronic reservoir (see Appendix A).

### C. The performance of the hybrid thermal machine for multiple tasks

We will show that the three-terminal configuration is sufficient to perform nontrivial multiple thermodynamic tasks [50]. First, work can be used to cool down the cold reservoir and warm up the hot reservoir (i.e.,  $I_Q^R > 0$ ,  $I_Q^{\text{ph}} < 0$ , and  $\dot{W} > 0$ ). Hence, the device simultaneously acts as a refrigerator and a heat pump. Specifically, using Eq. (2), the efficiency in this operation regime reads

$$\phi_{\text{PR}} = \frac{-I_Q^R A_Q^R - I_Q^{\text{ph}} A_Q^{\text{ph}}}{\dot{W}}, \quad (11)$$

where the subscript stands for *pump-refrigerator*. And the efficiency for producing work and cooling the cold reservoir (i.e.,  $I_Q^R > 0$ ,  $I_Q^{\text{ph}} > 0$ , and  $\dot{W} < 0$ ) is given by

$$\phi_{\text{ER}} = \frac{-I_Q^R A_Q^R - \dot{W}}{I_Q^{\text{ph}} A_Q^{\text{ph}}}. \quad (12)$$

While for heat engine and heat pump (i.e.,  $I_Q^R < 0$ ,  $I_Q^{\text{ph}} < 0$ , and  $\dot{W} < 0$ ), the corresponding efficiency is expressed

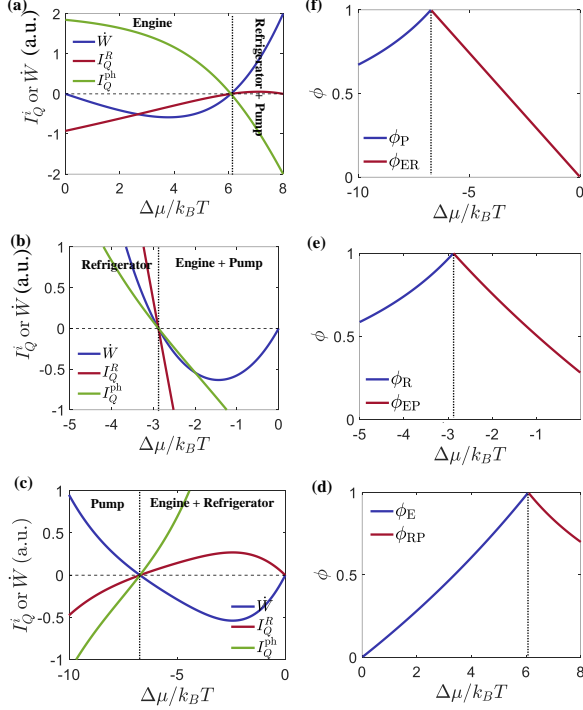


FIG. 3. Three-terminal double QD system performance. (a)-(c) Currents and power, and (d)-(f) efficiencies, as a function of the chemical potential difference  $\Delta\mu$  for simultaneous heating, cooling, and power production, where (a) and (d)  $E_L = 4k_B T$ ,  $E_R = -4k_B T$ , (b) and (e)  $E_L = 12k_B T$ ,  $E_R = 10k_B T$ , (c) and (f)  $E_L = -12k_B T$ ,  $E_R = 0$ . The other parameters are  $t = 0.15k_B T$ ,  $\gamma_l = \gamma_r = 0.4k_B T$ ,  $\gamma_{e-ph} = 0.1k_B T$ ,  $k_B T_R = k_B T$ ,  $k_B T_{ph} = 5.0k_B T$ ,  $k_B T_L = 1.5k_B T$  and  $k_B T = 10$  meV.

as

$$\phi_{EP} = \frac{-I_Q^{ph} A_Q^{ph} - \dot{W}}{I_Q^R A_Q^R}. \quad (13)$$

From the definitions in Eqs.(8)-(13), it is clear to find that the exergy efficiency better characterizes the function of thermal machine, compared with the convention thermodynamic efficiency [61, 62]. Moreover, we should point out the system is unable to simultaneously heat the hottest reservoir, cool the coldest reservoir, and produce work, which stems from the constraint by the second law of thermodynamics, i.e.,  $\phi \leq 1$  [70].

The versatility of this setup is manifested in Fig. 3. In particular, we consider the possibility of reproducing the hybrid configurations, e.g., engine-pump, engine-refrigerator, and refrigerator-pump. We include two separate contributions associated with two different tasks being performed simultaneously. Here we show how heat currents/output work [Fig. 3(a)-3(c)] as well as the corresponding efficiencies [Fig. 3(d)-3(f)] efficiently characterize thermodynamic multitask, with respect to the chem-

ical potential difference  $\Delta\mu$  [71]. Through varying  $\Delta\mu$ , we find the operation switch between a hybrid regime and the complementary single-task regime. Based on Eqs. (5) and (6), the corresponding vanishing position for currents, termed the current cutoff voltage, can be obtained as  $I_p^R \approx 0$ . For example, in Fig. 3(d), we see that when  $0 < \Delta\mu < 6k_B T$ , the device produces powers to the reservoirs, which performs the task of being a heat engine  $\dot{W} > 0$  (see the blue line). As  $\Delta\mu > 6k_B T$ , the device will heat the hottest reservoir  $I_Q^{ph} < 0$  and cool the coldest reservoir  $I_Q^R > 0$ , which acts as hybrid thermal machines. In analogy, we see a similar behavior in Figs. 3(e) and 3(f). When  $\Delta\mu \approx -3k_B T$  ( $-7k_B T$ ), the device will change from a single task of the refrigerator (heat pump) to two simultaneous tasks of heat engine and heat pump (engine and refrigerator).

We also note that thermodynamic laws set a bound on the efficiency of the quantum thermal machine, where the output work and efficiency cannot be maximized simultaneously. Such restriction refers to the power-efficiency trade-off [13, 15, 58, 72–75], e.g., the operating efficiency reaching the unit and the output work vanishing. In addition to the above functions, our three-terminal setups characterized as Eq. (9) can also be designed for cooling by heating processes. As proposed by Cleuren *et al.*[35], the chemical potential difference is kept zero and the coolest electronic reservoir is cooled by the hot phonon bath.

#### D. Linear transport and thermoelectric cooperative effect

Until now, we focus on the thermoelectric energy conversion efficiency of the three-terminal quantum thermal machine, of which two main parameters for characterizing thermodynamic performance are the figure of merit  $\xi$  and power factor  $P$ . Next, we demonstrate in detail how the cooperative effect can improve the exergy efficiency (figure of merit) in the linear response regime.

Based on Eqs. (5) and (6), the transport equations are reexpressed as [33, 34, 60]

$$\begin{pmatrix} I_p^R \\ I_Q^R \\ I_Q^{ph} \end{pmatrix} = \begin{pmatrix} M_{11} & M_{12} & M_{13} \\ M_{12} & M_{22} & M_{23} \\ M_{13} & M_{23} & M_{33} \end{pmatrix} \begin{pmatrix} A_p^R \\ A_Q^R \\ A_Q^{ph} \end{pmatrix}, \quad (14)$$

where the Onsager coefficients  $M_{ij} = M_{ij}^{el} + M_{ij}^{inel}$  include both the elastic and inelastic transport components [63]. Moreover, the second law of thermodynamics, i.e.,  $dS/dt \geq 0$  [66], leads to

$$\begin{aligned} M_{11}, M_{22}, M_{33} &\geq 0, & M_{11}M_{22} &\geq M_{12}^2, \\ M_{11}M_{33} &\geq M_{13}^2, & M_{22}M_{33} &\geq M_{23}^2. \end{aligned} \quad (15)$$



And the determinant of the transport matrix in Eq. (14) should be non-negative.

For systems with time-reversal symmetry, the maximal efficiency and maximal power of the three-terminal devices are expressed as

$$\phi_{\max} = \frac{\sqrt{\xi+1}-1}{\sqrt{\xi+1}+1}, \quad W_{\max} = \frac{1}{4}PT^2, \quad (16)$$

where  $\xi$  is the dimensionless figure of merit and  $P$  is the power factor, respectively [76]. The maximal efficiency quantifies the performance of hybrid thermal machines, including heat engines, refrigerators, heat pumps and their combinations. Clearly,  $\phi_{\max}$  approaches the unit when  $\xi$  approaches  $\infty$ .

Alternatively from the geometric perspective, the two temperatures can be parametrized as [60–62, 77, 78]  $A_Q^R = T_A \cos \theta$ , and  $A_Q^{\text{ph}} = T_A \sin \theta$ . Consequently, the figure of merit and power factor are described as

$$\frac{1}{\xi(\theta)} = \frac{M_{22} \cos^2 \theta + 2M_{23} \sin \theta \cos \theta + M_{33} \sin^2 \theta}{M_{11}(S_1 \cos \theta + S_2 \sin \theta)^2} - 1, \quad (17)$$

$$P(\theta) = M_{11}(S_1 \cos \theta + S_2 \sin \theta)^2. \quad (18)$$

where  $S_1 = M_{12}/M_{11}$  and  $S_2 = M_{13}/M_{11}$  denote the longitudinal and transverse thermopowers, respectively. Using Eqs. (17) and (18), it is straightforward to obtain the expressions of the longitudinal ( $\theta = 0$  or  $\pi$ ) and transverse ( $\theta = \pi/2, 3\pi/2$ ) figure of merit and power factor. The details can be found in Table I, where  $\mathcal{M} = M_{11}M_{22}M_{33} - M_{11}M_{23}^2 - M_{33}M_{12}^2 + 2M_{12}M_{13}M_{23} - M_{22}M_{13}^2$ . Specifically, we find that  $\xi_{\max} \geq \max(\xi_L, \xi_T)$  and  $P_{\max} \geq \max(P_L, P_T)$ .

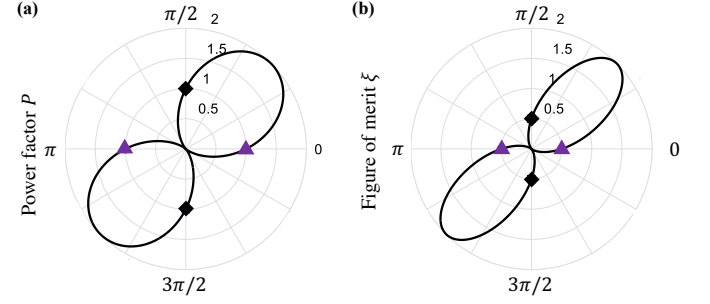


FIG. 4. Polar plot of (a) power factor  $P(\theta)$  and (b) figure of merit  $\xi(\theta)$  [in arbitrary unit (a.u.)] versus angle  $\theta$ . At  $\theta = 0$  or  $\pi$ ,  $\xi$  and  $P$  recover the values for the longitudinal thermoelectric effect (purple triangles,  $\xi_L$  and  $P_L$ ), while at  $\theta = \pi/2$  and  $3\pi/2$ , they recover the transverse thermoelectric effect (black rhombus,  $\xi_T$  and  $P_T$ ). The parameters are same with Fig. 3.

TABLE I. Longitudinal and transverse thermoelectric effects and their maximum

Performance	Figure of merit	Power factor
Longitudinal	$\xi_L = \frac{M_{11}S_1^2}{M_{22}-M_{11}S_1^2}$	$P_L = M_{11}S_1^2$
Transverse	$\xi_T = \frac{M_{11}S_2^2}{M_{33}-M_{11}S_2^2}$	$P_T = M_{11}S_2^2$
Maximum	$\xi_{\max} = \frac{M_{33}M_{12}^2 - 2M_{12}M_{13}M_{23} + M_{22}M_{13}^2}{\mathcal{M}}$	$P_{\max} = M_{11}(S_1^2 + S_2^2)$

Figure 4 shows the figure of merit  $\xi$  and power factor  $P$  by tuning the angle  $\theta$  in a polar plot. We demonstrate the robustness of the cooperative effects by examining the renormalized factor of power  $P_{\max}/\max(P_L, P_T)$  and the renormalized factor of efficiency  $\xi_{\max}/\max(\xi_L, \xi_T)$ . Outstandingly, the maximum figure of merit  $\xi_{\max}$  can be greater than the longitudinal figure of merit  $\xi_L$  (the purple triangle in Fig. 4(b)) and transverse one  $\xi_T$  (the black rhombus in Fig. 4(b)) for  $0 < \theta < \pi/2$  and  $\pi < \theta < 3\pi/2$ . In order to further understand the physical mechanism of thermoelectric cooperation effect, we know from Eq. (14) that the particle current is expressed as  $I_p^R = M_{11}A_p^R + M_{12}A_Q^R + M_{13}A_Q^{\text{ph}}$ , where  $M_{12}A_Q^R$  represents the longitudinal thermoelectric effect and  $M_{13}A_Q^{\text{ph}}$

represents the transverse one. As  $0 < \theta < \pi/2$  and  $\pi < \theta < 3\pi/2$ , it is found that  $(M_{12}A_Q^R) \times (M_{13}A_Q^{\text{ph}}) > 0$  and the longitudinal and transverse thermoelectric effects are coherently superposed. The similar physical effect can be found for the power factor. Therefore, we conclude that the thermoelectric figure of merit and power factor can be enhanced by exploiting cooperative effects.

### III. THE FOUR-TERMINAL THERMOELECTRIC QD SYSTEMS

To further illustrate the functionality of inelastic hy-

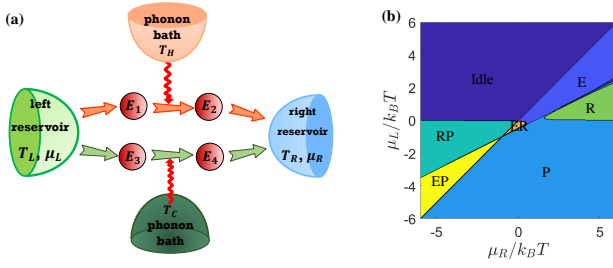


FIG. 5. (a) Schematic of four-terminal four-QD thermoelectric systems. The left reservoir and right reservoir with chemical potentials  $\mu_{L/R}$  and temperatures  $T_{L/R}$  connects with the central QD systems, in which there are two parallel transport channels: the upper channel has two QDs (with energies  $E_1$  and  $E_2$ ) and a phonon bath  $H$  (with temperature  $T_H$ ); the lower channel has two QDs (with energies  $E_3$  and  $E_4$ ) and a phonon bath  $C$  (with temperature  $T_C$ ). The two channels are spatially separated so that the phonon bath  $H$  ( $C$ ) couples only to the upper (lower) channel. (b) Map of the system functionality as the functions of the chemical potentials  $\mu_L$  and  $\mu_R$ . The parameters are:  $E_1 = 2.0k_B T$ ,  $E_2 = 0$ ,  $E_3 = 1.0k_B T$ ,  $E_4 = 5.0k_B T$ ,  $\gamma_{e-ph} = 0.1k_B T$ ,  $k_B T_L = k_B T$ ,  $k_B T_C = 0.7k_B T$ ,  $k_B T_H = 2.0k_B T$ ,  $k_B T_R = 0.5k_B T$ , and  $k_B T = 10 \text{ meV}$ .

brid thermal machines, we consider another typical thermoelectric transport model, i.e., four-terminal thermoelectric QD systems. In Ref. [79], we studied a unconventional inelastic thermoelectric effect, termed as cooling by transverse heat current effect. It describes the cooling process of the source driven by the heat exchange between the two thermal baths, rather than total heat injected into the central quantum system [35]. In this section, we study how to use the temperature gradient to overcome the chemical potential different to generate useful work (heat engines), or use the chemical potential to against the temperature bias to generate the heat current from the hot reservoir to cold one (refrigerators and/or heat pumps). Interestingly, this device performs multiple useful tasks simultaneously, which demonstrates that more thermodynamic forces enrich the implementation of hybrid operations.

The mesoscopic four-terminal thermoelectric devices coupled with two electric reservoirs and two phononic reservoirs as depicted in Fig. 5(a). The system consists of four QDs: QD 1 and QD 2 with the energies  $E_1$  and  $E_2$  in the upper channel are coupled with the hot phononic reservoir  $H$ , while QD 3 and QD 4 in the lower channel with energy  $E_3$  and  $E_4$  are connected with the cold phononic bath  $C$ . The inelastic-scattering processes dominate the thermoelectric transport [80, 81].  $I_p^i$  ( $i = L, R$ ) is the particle current flowing from the reser-

voir  $i$  into system and  $I_Q^i$  ( $i = L, R, H, C$ ) is the heat current flows from the reservoir  $i$  into the system.

Due to energy conservation ( $I_Q^L + \mu_L I_p^L + I_Q^H + I_Q^C + I_Q^R + \mu_R I_p^R = 0$ ) and particle conservation ( $I_p^L + I_p^R = 0$ ), the entropy production rate of the whole system is given by [79]

$$T_L \frac{dS}{dt} = I_p^R X_p^R + I_Q^R X_Q^R + I_Q^H X_Q^H + I_Q^C X_Q^C, \quad (19)$$

where the affinities are defined as  $X_p^R = \mu_R - \mu_L$ ,  $X_Q^R = 1 - \frac{T_L}{T_R}$ ,  $X_Q^C = 1 - \frac{T_L}{T_C}$ ,  $X_Q^H = 1 - \frac{T_L}{T_H}$ . Here, we restrict our discussion where there is only one energy level in each QD. In this setup, the phonon-assisting particle currents through two independent upper and lower channels are described as [64],

$$I_{\text{up}} = \Gamma_{1 \rightarrow 2} - \Gamma_{2 \rightarrow 1}, \quad I_{\text{down}} = \Gamma_{3 \rightarrow 4} - \Gamma_{4 \rightarrow 3} \quad (20)$$

where  $\Gamma_{i \rightarrow j}$  is the electron tunneling rate from QD  $i$  to QD  $j$  [79]. Then, the particle and heat currents derived from the Fermi golden rule [63] can be written as

$$\begin{aligned} I_p^L &= I_{\text{up}} + I_{\text{down}}, & I_Q^L &= (E_1 - \mu_L)I_{\text{up}} + (E_3 - \mu_L)I_{\text{down}}, \\ I_Q^R &= -(E_2 - \mu_R)I_{\text{up}} - (E_4 - \mu_R)I_{\text{down}}, \\ I_Q^H &= (E_2 - E_1)I_{\text{up}}, & I_Q^C &= (E_4 - E_3)I_{\text{down}}. \end{aligned} \quad (21)$$

And the output power of the device  $-\dot{W}$  is given by

$$\dot{W} = I_p^R \Delta\mu, \quad (22)$$

where  $\Delta\mu = \mu_R - \mu_L \equiv X_p^R$  is the chemical potential difference. In this four-terminal systems, we set the temperatures as

$$T_R < T_C < T_L < T_H. \quad (23)$$

The definitions of efficiency for the four-terminal device in different operation regimes are shown in Table II. In our setup, heating the hottest reservoir and cooling the coolest reservoir are considered as useful processes, and this part of entropy production is reduced. In contrast, heating or cooling an intermediate temperature heat reservoir is considered as a useless process. In the situation with  $X_p^R = 0$  and  $T_C = (2/T_L - 1/T_H)^{-1}$ , the efficiency of refrigerators is simplified as  $\phi = -(2I_Q^R)/(I_Q^H - I_Q^C)$ . It is convenient to discover a mode of cooling by transverse heat current effect: the coolest right reservoir can be cooled by passing a heat current between the  $H$  phonon bath and the  $C$  phonon bath, with no energy exchange between the phonon and electronic reservoirs [79, 81]. Obviously, the cooling by thermal current operation requires a higher temperature of phonon bath than the cooling by electric power. Hence, we mainly consider the latter situation when the temperature gradient is comparatively small.

TABLE II. Functionality of four-terminal four-QD thermal machine

Thermal progresses	work and heat currents	Efficiency
Heat engine	$I_Q^R < 0, I_Q^H > 0, \dot{W} < 0, I_Q^C < 0$	$\phi_E = \frac{-\dot{W}}{I_Q^R X_Q^R + I_Q^C X_Q^C + I_Q^H X_Q^H}$
Heat pump	$I_Q^H < 0, I_Q^R < 0, \dot{W} > 0, I_Q^C < 0$	$\phi_P = \frac{-I_Q^H X_Q^H}{I_Q^R X_Q^R + I_Q^C X_Q^C + \dot{W}}$
Refrigerator	$I_Q^R > 0, I_Q^H > 0, \dot{W} > 0, I_Q^C < 0$	$\phi_R = \frac{-I_Q^R X_Q^R}{I_Q^H X_Q^H + I_Q^C X_Q^C + \dot{W}}$
Refrigerator and heat pump	$I_Q^R > 0, I_Q^H < 0, \dot{W} > 0, I_Q^C < 0$	$\phi_{PR} = \frac{-I_Q^R X_Q^R - I_Q^H X_Q^H}{I_Q^C X_Q^C + \dot{W}}$
Engine and refrigerator	$I_Q^R > 0, I_Q^H > 0, \dot{W} < 0, I_Q^C < 0$	$\phi_{ER} = \frac{-I_Q^R X_Q^R - \dot{W}}{I_Q^H X_Q^H + I_Q^C X_Q^C}$
Engine and heat pump	$I_Q^R < 0, I_Q^H < 0, \dot{W} < 0, I_Q^C < 0$	$\phi_{EP} = \frac{-I_Q^H X_Q^H - \dot{W}}{I_Q^R X_Q^R + I_Q^C X_Q^C}$

Fig. 5(b) displays all possible functionalities for the thermal machines, and the change of current symbol means the realization of different functions, by tuning the chemical potential of left ( $\mu_L$ ) and right ( $\mu_R$ ) reservoirs. From this map figure, we observe that the four-terminal device can realize any functions and perform different tasks by adjusting physical parameters.

In order to emphasize the role of thermodynamic biases in the four-terminal system, we compare the performance of such setup at  $T_L = T_R$  with the case  $T_L \neq T_R$  for the same three-terminal quantum-dot thermal machines in Fig. 6. We first show the efficiency of the thermal machines in Figs. 6(a)-6(c), which exhibits two useful tasks as functions of QD energy  $E_1$  and chemical potential  $\mu_L$ , and the efficiency can even reach the unity in some parameter regions. In Fig. 6(d)-6(f), we compare the above two cases and it is easy to find that the max-

imum efficiency can be significantly improved when the four-terminal device goes from the condition of  $T_L = T_R$  to  $T_L \neq T_R$ . Through concrete numerical results, we find that the setup with multiple biases can substantially enlarge the parameter region of the high efficiency, and thus provide a promising pathway toward high-performance thermal machines.

Finally, we point out that there are three Seebeck coefficients induced by three temperature gradients, which originate from the three thermal affinities,  $X_Q^R$ ,  $X_Q^H$ , and  $X_Q^C$  in the linear-response regime for the four-terminal thermoelectric device. Correspondingly, the figures of merit refer to the conventional longitudinal thermoelectric effects and the unconventional transverse thermoelectric effects, respectively. The high figure of merit for unconventional thermoelectric effects require the small variance of the phonon energy, but the electron energy variance.

#### IV. CONCLUSIONS

In this work, a general thermodynamic efficiency, termed as “exergy efficiency”, was defined from an entropic point of view, which can characterize the functions of the thermal machines, such as heat engine, refrigerator, and heat pump, without the need to specifically define a reference temperature. The exergy efficiency is appointed for each functionality as the ratio of the output (the consumed usable energy) to the consumed (the target heat).

We discussed thermodynamic operations of phonon-thermoelectric device that perform multiple useful tasks simultaneously in two typical thermoelectric systems [(i) devices with two electronic and a phonon terminals, (ii) those with two electronic terminals and two phononic ter-

minals], where phonon-assisted inelastic processes dominate the transport. In the three-terminal device, we found the parameter region and the corresponding exergy efficiency of the thermal machines for power production, cooling, heating, and the simultaneous combinations. It is found that a hybrid thermal machine can be realized only if inelastic processes are taken into account. While in the four-terminal device, in addition to demonstrating that the device can perform two useful tasks, we further emphasized the improvement of exergy efficiency by multiple thermodynamic biases.

Moreover, in the linear-response regime, from the geometric aspect we demonstrated that the thermoelectric cooperative effects can enhance the performance of multi-tasks, e.g., efficiency and output power, which are tightly related with the figure of merit and power factor. Due to the inelastic thermoelectric effect, particle and heat



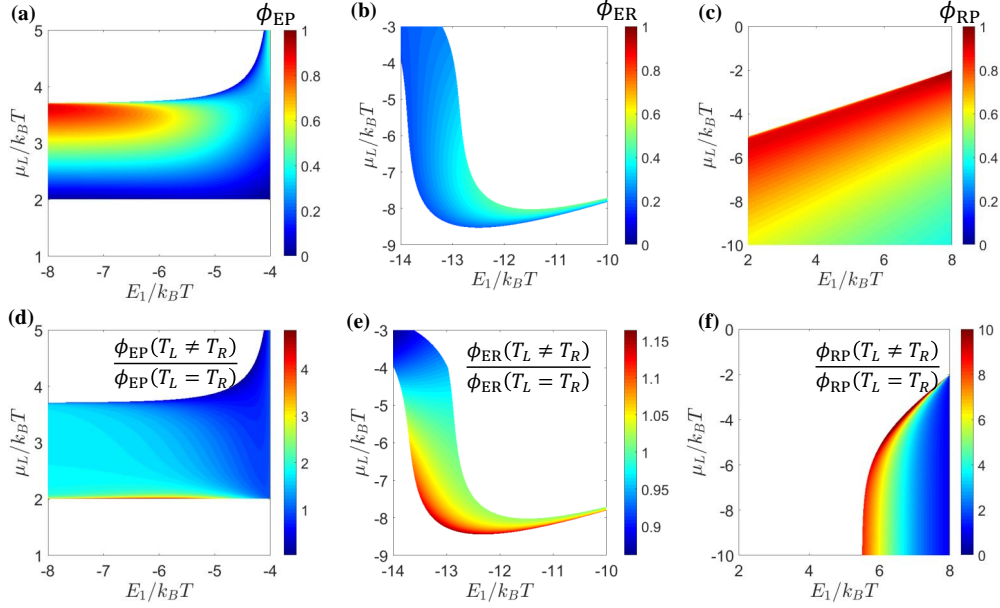


FIG. 6. The efficiencies of hybrid thermal machines (a)  $\phi_{EP}$ , (b)  $\phi_{ER}$  and (c)  $\phi_{RP}$  as the functions of the chemical potential  $\mu_L$  and QD energy  $E_1$  for  $T_C = 0.7k_BT$ . (d)-(f) Comparing the efficiency for  $T_L \neq T_C$  case and the  $T_L = T_C$  as the functions of the chemical potential  $\mu_L$  and QD energy  $E_1$ . The parameters: (a) and (d)  $E_2 = -4.0k_BT$ ,  $E_3 = 2.0k_BT$ ,  $E_4 = -1.0k_BT$ . (b) and (e)  $E_2 = 6.0k_BT$ ,  $E_3 = 6.0k_BT$ ,  $E_4 = 8.0k_BT$ . (c) and (f)  $E_2 = 8.0k_BT$ ,  $E_3 = 6.0k_BT$ ,  $E_4 = -4.0k_BT$ . The other parameters are  $\gamma_{e-ph} = 0.1k_BT$ ,  $k_BT_L = k_BT$ ,  $k_BT_H = 2.0k_BT$ ,  $k_BT_R = 0.5k_BT$ , and  $k_BT = 10$  meV. The white region indicates the function of the hybrid thermal machines is not performed.

currents can flow in spatially separated parts of the multiterminal systems. Our analytical results revealed the importance of inelastic transport effects for the design of the high performance thermoelectric device.

Finally, it should be pointed out that our study is based on the steady-state transport. The performance of the periodically driven thermoelectric device with inelastic transport undertaking multitasks is fascinating in future study.

## V. ACKNOWLEDGEMENTS

We are grateful to Professor Jie Ren for many interesting discussions. This work was supported by the funding for the National Natural Science Foundation of China under Grants No. 12125504, No. 12074281, and No. 11704093, the Opening Project of Shanghai Key Laboratory of Special Artificial Microstructure Materials and Technology, and Jiangsu Key Disciplines of the Fourteenth Five-Year Plan (Grant No. 2021135).

## Appendix A: The hybrid thermal machines: three-terminal single-level QD System

In this appendix, we study the operation and performance of the elastic thermoelectric devices that perform multiple useful tasks simultaneously. In our construction (see Fig. 7)(a), a single QD system exchanges particle and energy with three electronic reservoirs,  $L$ ,  $R$ , and  $P$ . The particle and heat currents flowing from the reservoir into the system are expressed as[65]

$$I_p^L = \sum_{i=R,P} \frac{\Gamma_i \Gamma_L [f_L(E_0) - f_i(E_0)]}{\Gamma_L + \Gamma_i}, \quad (A1a)$$

$$I_p^R = \sum_{i=L,P} \frac{\Gamma_i \Gamma_R [f_R(E_0) - f_i(E_0)]}{\Gamma_R + \Gamma_i}, \quad (A1b)$$

$$I_p^P = \sum_{i=L,R} \frac{\Gamma_i \Gamma_P [f_P(E_0) - f_i(E_0)]}{\Gamma_P + \Gamma_i}, \quad (A1c)$$

and

$$I_Q^L = \sum_{i=R,P} \frac{(E_0 - \mu_L) \Gamma_i \Gamma_L [f_L(E_0) - f_i(E_0)]}{\Gamma_L + \Gamma_i}, \quad (A2a)$$

$$I_Q^R = \sum_{i=L,P} \frac{(E_0 - \mu_R) \Gamma_i \Gamma_R [f_R(E_0) - f_i(E_0)]}{\Gamma_R + \Gamma_i}, \quad (A2b)$$

$$I_Q^P = \sum_{i=L,R} \frac{(E_0 - \mu_P) \Gamma_i \Gamma_P [f_P(E_0) - f_i(E_0)]}{\Gamma_P + \Gamma_i}, \quad (A2c)$$

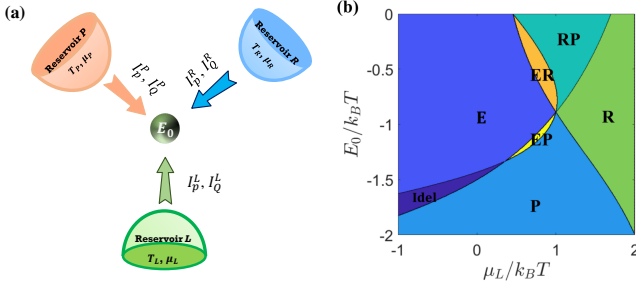


FIG. 7. (a) Schematic figure of a three-terminal single-QD thermoelectric device. The QD with a single energy level  $E_0$  are connected in series to three fermionic reservoirs  $i$  ( $i = L, R, P$ ). The chemical potential and temperature of reservoirs are  $\mu_i$  and  $T_i$ . The constant  $\Gamma$  represents the coupling between the QD and reservoir. (b) Map of the system efficiency as the functions of the chemical potential  $\mu_L$  and QD energy  $E_0$ . The parameters are  $\mu_R = 0$ ,  $\mu_P = 2.0k_B T$ .

respectively. Particle conservation implies that  $I_P^L + I_P^R + I_P^P = 0$ , while energy conservation requires  $I_Q^L + \mu_L I_P^L + I_Q^R + \mu_R I_P^R + I_Q^P + \mu_P I_P^P = 0$  [2].

Considering the energy and particle conversations, the entropy production is given by a specific form,

$$T_L \frac{dS}{dt} = F_P^R I_P^R + F_P^P I_P^P + F_Q^R I_Q^R + F_Q^P I_Q^P. \quad (A3)$$

where  $F_P^R = \mu_R - \mu_L$ ,  $F_P^P = \mu_P - \mu_L$ ,  $F_Q^R = 1 - \frac{T_L}{T_R}$ , and  $F_Q^P = 1 - \frac{T_L}{T_P}$ .

The power done by the reservoirs to the system is given by [61]

$$\dot{W} = F_P^R I_P^R + F_P^P I_P^P, \quad (A4)$$

and in the single QD three-terminal systems, we set

$$T_R < T_L < T_P, \quad (A5)$$

and choose the temperature of the left reservoir as the reference temperature. The exergy efficiency in six different operational regimes is shown in Table III. In Fig. 7(b), we find the device with three electronic reservoirs also can perform useful multitasks through adjusting the QD energy  $E_0$  and chemical potential  $\mu_L$ .

TABLE III. Functionality of three-terminal single-QD thermal machine

Thermal progresses	work and heat currents	Efficiency
Heat engine	$I_Q^R < 0, I_Q^P > 0, \dot{W} < 0$	$\phi_E = \frac{-\dot{W}}{I_Q^R F_Q^R + I_Q^P F_Q^P}$
Heat pump	$I_Q^P < 0, I_Q^R < 0, \dot{W} > 0$	$\phi_P = \frac{-I_Q^P F_Q^P}{I_Q^R F_Q^R + \dot{W}}$
Refrigerator	$I_Q^R > 0, I_Q^P > 0, \dot{W} > 0$	$\phi_R = \frac{-I_Q^R F_Q^R}{I_Q^P F_Q^P + \dot{W}}$
Refrigerator and pump	$I_Q^R > 0, I_Q^P < 0, \dot{W} > 0$	$\phi_{PR} = \frac{-I_Q^R F_Q^R - I_Q^P F_Q^P}{\dot{W}}$
Engine and refrigerator	$I_Q^R > 0, I_Q^P > 0, \dot{W} < 0$	$\phi_{ER} = \frac{-I_Q^R F_Q^R - \dot{W}}{I_Q^P F_Q^P}$
Engine and pump	$I_Q^R < 0, I_Q^P < 0, \dot{W} < 0$	$\phi_{EP} = \frac{-I_Q^P F_Q^P - \dot{W}}{I_Q^R F_Q^R}$

[1] B. Sothmann, R. Sánchez, and A. N. Jordan, “Thermoelectric energy harvesting with quantum dots,” *Nanotechnology* **26**, 032001 (2015).  
[2] J.-H. Jiang and Y. Imry, “Linear and nonlinear mesoscopic thermoelectric transport with coupling with heat baths,” *C. R. Phys.* **17**, 1047 – 1059 (2016).  
[3] G. Benenti, G. Casati, K. Saito, and R. S. Whitney, “Fundamental aspects of steady-state conversion of heat to work at the nanoscale,” *Phys. Rep.* **694**, 1 – 124 (2017).  
[4] J. P. Pekola and B. Karimi, “Colloquium: Quantum heat transport in condensed matter systems,” *Rev. Mod.*

*Phys.* **93**, 041001 (2021).  
[5] R. Wang, C. Wang, J. Lu, and J.-H. Jiang, “Inelastic thermoelectric transport and fluctuations in mesoscopic systems,” *Adv. Phys.: X* **7**, 2082317 (2022).  
[6] V. Mukherjee and U. Divakaran, “Many-body quantum thermal machines,” *J. Phys.: Condens. Matter* **33**, 454001 (2021).  
[7] R. S. Whitney, “Most efficient quantum thermoelectric at finite power output,” *Phys. Rev. Lett.* **112**, 130601 (2014).  
[8] R. S. Whitney, “Finding the quantum thermoelectric with maximal efficiency and minimal entropy production

- at given power output,” *Phys. Rev. B* **91**, 115425 (2015).
- [9] O. Entin-Wohlman, J.-H. Jiang, and Y. Imry, “Efficiency and dissipation in a two-terminal thermoelectric junction, emphasizing small dissipation,” *Phys. Rev. E* **89**, 012123 (2014).
- [10] M. Josefsson, A. Svilans, H. Linke, and M. Leijnse, “Optimal power and efficiency of single quantum dot heat engines: Theory and experiment,” *Phys. Rev. B* **99**, 235432 (2019).
- [11] R.-X. Zhai, F.-M. Cui, Y.-H. Ma, C. P. Sun, and H. Dong, “Experimental implementation of finite-time carnot cycle,” [arXiv:2206.10153](https://arxiv.org/abs/2206.10153) (2022).
- [12] K. Proesmans, B. Cleuren, and C. Van den Broeck, “Power-efficiency-dissipation relations in linear thermodynamics,” *Phys. Rev. Lett.* **116**, 220601 (2016).
- [13] N. Shiraishi, K. Saito, and H. Tasaki, “Universal trade-off relation between power and efficiency for heat engines,” *Phys. Rev. Lett.* **117**, 190601 (2016).
- [14] B.-q. Guo, T. Liu, and C.-s. Yu, “Multifunctional quantum thermal device utilizing three qubits,” *Phys. Rev. E* **99**, 032112 (2019).
- [15] P. Pietzonka and U. Seifert, “Universal trade-off between power, efficiency, and constancy in steady-state heat engines,” *Phys. Rev. Lett.* **120**, 190602 (2018).
- [16] Y.-H. Ma, R.-X. Zhai, J. Chen, C. P. Sun, and H. Dong, “Experimental test of the  $1/\tau$ -scaling entropy generation in finite-time thermodynamics,” *Phys. Rev. Lett.* **125**, 210601 (2020).
- [17] Y.-Q. Liu, D.-H. Yu, and C.-S. Yu, “Common environmental effects on quantum thermal transistor,” *Entropy* **24** (2022), 10.3390/e24010032.
- [18] G. D. Mahan and J. O. Sofo, “The best thermoelectric,” *Proc. Natl. Acad. Sci. USA* **93**, 7436–7439 (1996).
- [19] J. Zhou, R. Yang, G. Chen, and M. S. Dresselhaus, “Optimal bandwidth for high efficiency thermoelectrics,” *Phys. Rev. Lett.* **107**, 226601 (2011).
- [20] F. Mazza, S. Valentini, R. Bosisio, G. Benenti, V. Giovannetti, R. Fazio, and F. Taddei, “Separation of heat and charge currents for boosted thermoelectric conversion,” *Phys. Rev. B* **91**, 245435 (2015).
- [21] O. Entin-Wohlman, Y. Imry, and A. Aharony, “Three-terminal thermoelectric transport through a molecular junction,” *Phys. Rev. B* **82**, 115314 (2010).
- [22] D. Sánchez and R. López, “Scattering theory of nonlinear thermoelectric transport,” *Phys. Rev. Lett.* **110**, 026804 (2013).
- [23] J.-H. Jiang, O. Entin-Wohlman, and Y. Imry, “Three-terminal semiconductor junction thermoelectric devices: improving performance,” *New J. Phys.* **15**, 075021 (2013).
- [24] B. Sothmann, R. Sánchez, A. N Jordan, and M. Büttiker, “Powerful energy harvester based on resonant-tunneling quantum wells,” *New J. Phys.* **15**, 095021 (2013).
- [25] K. Yamamoto, O. Entin-Wohlman, A. Aharony, and N. Hatano, “Efficiency bounds on thermoelectric transport in magnetic fields: The role of inelastic processes,” *Phys. Rev. B* **94**, 121402 (2016).
- [26] Y. Zhang, G. Lin, and J. Chen, “Three-terminal quantum-dot refrigerators,” *Phys. Rev. E* **91**, 052118 (2015).
- [27] B. K. Agarwalla, J.-H. Jiang, and D. Segal, “Full counting statistics of vibrationally assisted electronic conduction: Transport and fluctuations of thermoelectric efficiency,” *Phys. Rev. B* **92**, 245418 (2015).
- [28] B. K. Agarwalla, J.-H. Jiang, and D. Segal, “Quantum efficiency bound for continuous heat engines coupled to noncanonical reservoirs,” *Phys. Rev. B* **96**, 104304 (2017).
- [29] L. Wang, Z. Wang, C. Wang, and J. Ren, “Cycle flux ranking of network analysis in quantum thermal devices,” *Phys. Rev. Lett.* **128**, 067701 (2022).
- [30] R. Sánchez and M. Büttiker, “Optimal energy quanta to current conversion,” *Phys. Rev. B* **83**, 085428 (2011).
- [31] H. Thierschmann, F. Arnold, M. Mittermüller, L. Maier, C. Heyn, W. Hansen, H. Buhmann, and L. W. Molenkamp, “Thermal gating of charge currents with coulomb coupled quantum dots,” *New J. Phys.* **17**, 113003 (2015).
- [32] S. M. Tabatabaei, D. Sánchez, Alfredo L. Yeyati, and R. Sánchez, “Andreev-coulomb drag in coupled quantum dots,” *Phys. Rev. Lett.* **125**, 247701 (2020).
- [33] J.-H. Jiang, O. Entin-Wohlman, and Y. Imry, “Thermoelectric three-terminal hopping transport through one-dimensional nanosystems,” *Phys. Rev. B* **85**, 075412 (2012).
- [34] J.-H. Jiang, O. Entin-Wohlman, and Y. Imry, “Hopping thermoelectric transport in finite systems: Boundary effects,” *Phys. Rev. B* **87**, 205420 (2013).
- [35] B. Cleuren, B. Rutten, and C. Van den Broeck, “Cooling by heating: Refrigeration powered by photons,” *Phys. Rev. Lett.* **108**, 120603 (2012).
- [36] J. Lu, R. Wang, J. Ren, M. Kulkarni, and J.-H. Jiang, “Quantum-dot circuit-qed thermoelectric diodes and transistors,” *Phys. Rev. B* **99**, 035129 (2019).
- [37] R. Kosloff and A. Levy, “Quantum heat engines and refrigerators: Continuous devices,” *Annu. Rev. Phys. Chem.* **65**, 365–393 (2014).
- [38] R. Wang, J. Lu, C. Wang, and J.-H. Jiang, “Nonlinear effects for three-terminal heat engine and refrigerator,” *Sci. Rep.* **8**, 2607 (2018).
- [39] D. Sánchez, R. Sánchez, R. López, and B. Sothmann, “Nonlinear chiral refrigerators,” *Phys. Rev. B* **99**, 245304 (2019).
- [40] J. Ren, P. Hänggi, and B. Li, “Berry-phase-induced heat pumping and its impact on the fluctuation theorem,” *Phys. Rev. Lett.* **104**, 170601 (2010).
- [41] Z. Wang, L. Wang, J. Chen, C. Wang, and J. Ren, “Geometric heat pump: Controlling thermal transport with time-dependent modulations,” *Front. Phys.* **17**, 1–14 (2022).
- [42] Z. Wang, J. Chen, and J. Ren, “Geometric heat pump and no-go restrictions of nonreciprocity in modulated thermal diffusion,” *Phys. Rev. E* **106**, L032102 (2022).
- [43] N. M. Myers, O. Abah, and S. Deffner, “Quantum thermodynamic devices: From theoretical proposals to experimental reality,” *AVS Quantum Sci.* **4**, 027101 (2022).

- [44] G. Manzano and R. Zambrini, “Quantum thermodynamics under continuous monitoring: A general framework,” *AVS Quantum Science* **4**, 025302 (2022).
- [45] Z.-C. Tu, “Abstract models for heat engines,” *Front. Phys.* **16**, 1–12 (2021).
- [46] J.-H. Jiang and Y. Imry, “Enhancing thermoelectric performance using nonlinear transport effects,” *Phys. Rev. Applied* **7**, 064001 (2017).
- [47] J.-H. Jiang and Y. Imry, “Near-field three-terminal thermoelectric heat engine,” *Phys. Rev. B* **97**, 125422 (2018).
- [48] J. Lu, Z. Wang, J. Peng, C. Wang, J.-H. Jiang, and J. Ren, “Geometric thermodynamic uncertainty relation in a periodically driven thermoelectric heat engine,” *Phys. Rev. B* **105**, 115428 (2022).
- [49] O. Entin-Wohlman, Y. Imry, and A. Aharony, “Enhanced performance of joint cooling and energy production,” *Phys. Rev. B* **91**, 054302 (2015).
- [50] G. Manzano, R. Sánchez, R. Silva, G. Haack, J. B. Brask, N. Brunner, and P. P. Potts, “Hybrid thermal machines: Generalized thermodynamic resources for multitasking,” *Phys. Rev. Research* **2**, 043302 (2020).
- [51] K. Hammam, H. Leitch, Y. Hassouni, and G. De Chiara, “Exploiting coherence for quantum thermodynamic advantage,” [arXiv:2202.07515](https://arxiv.org/abs/2202.07515) (2022).
- [52] G. T. Landi and M. Paternostro, “Irreversible entropy production: From classical to quantum,” *Rev. Mod. Phys.* **93**, 035008 (2021).
- [53] Thomas V. Marcella, “Entropy production and the second law of thermodynamics: An introduction to second law analysis,” *Am. J. Phys.* **60**, 888–895 (1992).
- [54] S. Mukherjee, B. De, and B. Muralidharan, “Three-terminal vibron-coupled hybrid quantum dot thermoelectric refrigeration,” *J. Appl. Phys.* **128**, 234303 (2020).
- [55] F. Hajiloo, R. Sánchez, R. S. Whitney, and J. Splettstoesser, “Quantifying nonequilibrium thermodynamic operations in a multiterminal mesoscopic system,” *Phys. Rev. B* **102**, 155405 (2020).
- [56] M. Carrega, L. M. Cangemi, G. De Filippis, V. Cataudella, G. Benenti, and M. Sassetti, “Engineering dynamical couplings for quantum thermodynamic tasks,” *PRX Quantum* **3**, 010323 (2022).
- [57] P. Strasberg and A. Winter, “First and second law of quantum thermodynamics: A consistent derivation based on a microscopic definition of entropy,” *PRX Quantum* **2**, 030202 (2021).
- [58] J.-H. Jiang, “Thermodynamic bounds and general properties of optimal efficiency and power in linear responses,” *Phys. Rev. E* **90**, 042126 (2014).
- [59] G. J. Snyder and T. S. Ursell, “Thermoelectric efficiency and compatibility,” *Phys. Rev. Lett.* **91**, 148301 (2003).
- [60] J.-H. Jiang, “Enhancing efficiency and power of quantum-dots resonant tunneling thermoelectrics in three-terminal geometry by cooperative effects,” *J. Appl. Phys.* **116**, 194303 (2014).
- [61] J. Lu, R. Wang, Y. Liu, and J.-H. Jiang, “Thermoelectric cooperative effect in three-terminal elastic transport through a quantum dot,” *J. Appl. Phys.* **122**, 044301 (2017).
- [62] Y. Liu, J. Lu, R. Wang, C. Wang, and J.-H. Jiang, “Energy cooperation in quantum thermoelectric systems with multiple electric currents,” *Chin. Phys. B* **29**, 40504 (2020).
- [63] J.-H. Jiang, M. Kulkarni, D. Segal, and Y. Imry, “Phonon thermoelectric transistors and rectifiers,” *Phys. Rev. B* **92**, 045309 (2015).
- [64] J. Lu, R. Wang, C. Wang, and J.-H. Jiang, “Brownian thermal transistors and refrigerators in mesoscopic systems,” *Phys. Rev. B* **102**, 125405 (2020).
- [65] G. Chen, *Nanoscale Energy Transport and Conversion* (Oxford University Press, London, 2005).
- [66] S. Datta, *Electronic transport in mesoscopic systems* (Cambridge university press, Cambridge, UK, 1995).
- [67] M. Esposito, K. Lindenberg, and C. Van den Broeck, “Thermoelectric efficiency at maximum power in a quantum dot,” *Europhys. Lett.* **85**, 60010 (2009).
- [68] O. Kedem and S. R. Caplan, “Degree of coupling and its relation to efficiency of energy conversion,” *Trans. Faraday Soc.* **61**, 1897–1911 (1965).
- [69] S. Saryal, M. Gerry, I. Khait, D. Segal, and B. K. Agarwalla, “Universal bounds on fluctuations in continuous thermal machines,” *Phys. Rev. Lett.* **127**, 190603 (2021).
- [70] P. Strasberg and A. Winter, “First and second law of quantum thermodynamics: A consistent derivation based on a microscopic definition of entropy,” *PRX Quantum* **2**, 030202 (2021).
- [71] V. Holubec and A. Ryabov, “Cycling tames power fluctuations near optimum efficiency,” *Phys. Rev. Lett.* **121**, 120601 (2018).
- [72] C. Van den Broeck, “Thermodynamic efficiency at maximum power,” *Phys. Rev. Lett.* **95**, 190602 (2005).
- [73] K. Proesmans, B. Cleuren, and C. Van den Broeck, “Power-efficiency-dissipation relations in linear thermodynamics,” *Phys. Rev. Lett.* **116**, 220601 (2016).
- [74] K. Brandner, K. Saito, and U. Seifert, “Thermodynamics of micro- and nano-systems driven by periodic temperature variations,” *Phys. Rev. X* **5**, 031019 (2015).
- [75] J. Lu, Y. Liu, R. Wang, C. Wang, and J.-H. Jiang, “Optimal efficiency and power, and their trade-off in three-terminal quantum thermoelectric engines with two output electric currents,” *Phys. Rev. B* **100**, 115438 (2019).
- [76] R. S. Whitney and K. Saito, “Thermoelectric coefficients and the figure of merit for large open quantum dots,” *SciPost Phys.* **6**, 12 (2019).
- [77] W. Niedenzu and G. Kurizki, “Cooperative many-body enhancement of quantum thermal machine power,” *New J. Phys.* **20**, 113038 (2018).
- [78] J. C. Lu, F. J. Zhuo, Z. Z. Sun, and J. H. Jiang, “Cooperative spin caloritronic devices,” *ES Energy. Environ.* **7**, 17–28 (2019).
- [79] J. Lu, J.-H. Jiang, and Y. Imry, “Unconventional four-terminal thermoelectric transport due to inelastic transport: Cooling by transverse heat current, transverse thermoelectric effect, and maxwell demon,” *Phys. Rev. B* **103**, 085429 (2021).
- [80] R. S. Whitney, R. Sánchez, F. Haupt, and J. Splettstoesser, “Thermoelectricity without absorbing

- energy from the heat sources,” [Physica E \*\*75\*\*, 257 – 265 \(2016\)](#).
- [81] M. Xi, R. Wang, J. Lu, and J.-H. Jiang, “Coulomb thermoelectric drag in four-terminal mesoscopic quantum transport,” [Chin. Phys. Lett. \*\*38\*\*, 088801 \(2021\)](#).